MACHINING SCIENCE AND TECHNOLOGY, 3(2), 255–271 (1999)

DUCTILE-REGIME MACHINING OF PARTICLE-REINFORCED METAL MATRIX COMPOSITES

N.P. Hung,[1] T.C. Tan,[2] Z.W. Zhong,[3] and G.W. Yeow[4]

[1,4]School of Mechanical & Production Engineering, Nanyang Tech. University, Singapore
[2]Hewlett Packard Singapore Pte Ltd, Singapore
[3]Gintic Institute of Manufacturing Technology, Singapore

Received September 29, 1998; Accepted June 28, 1999

ABSTRACT

This paper presents research results on ultraprecision machining of metal matrix composite (MMC) composed of aluminum matrix and either SiC or Al_2O_3 particles. Ductile-regime machining of both SiC and aluminum was evaluated to improve the surface integrity of the composite. Both polycrystalline diamond (PCD) and single crystalline diamond (SCD) tools were used to ultraprecision machine the composites at a depth of cut ranging from 0 to 1 μm using a taper cut. The feedrate was normalized to the tool nose radius. A model is proposed to calculate the critical depth of cut for MMCs reinforced with either Al_2O_3 or SiC. The critical depths of cut were found to be 1 μm and 0.2 μm for MMCs reinforced with Al_2O_3 or SiC, respectively. Both depth of cut and crystallographic direction of the ceramic particles are the sufficient conditions for ductile-regime machining. Although both tools produce similar surface finish, a SCD tool removed the MMC as chips while a PCD tool simply smeared the surface. A diffusion-abrasion mechanism was suspected to cause the surprising wear of the SCD tools when machining the aluminum/SiC composite.

INTRODUCTION

The nomenclature of Metal Matrix Composites (MMCs) used in this paper follows the ANSI/ASC H35.5-1992 recommendation. It includes the matrix, the reinforcement, the volume fraction of reinforcement, the type of reinforcement, and any additional secondary process. Thus, the 6061/SiC/20w-T6 composite consists of 6061 aluminum matrix, is reinforced with 20 vol % of SiC whisker, and is aged to a T6 temper.

Metal matrix composites were known for their synergistic properties; however, sensitive cost and fabrication challenges including machining were to be overcome for successful applications of these composites. The surface finish and surface integrity were important for surface sensitive parts such as optical lenses or parts subjected to fatigue or creep. Subsurface damages due to machining processes of MMCs resulted from conventional and unconventional processes such as in turning, milling, facing, drilling, electrical discharge machining, abrasive jet machining, laser machining, etc. (1–3). Literature surveys showed that finishing processes such as grinding and abrasive blasting were utilized to marginally improve the surface integrity of machined MMC samples (4, 5). Despite the research efforts, fracture of the brittle ceramic reinforcement in MMCs due to machining was still a serious challenge to manufacturing engineers and required further study. Ultraprecision machining was investigated as an alternative technique for finish machining. This project studied how ultraprecision machining affected the surface integrity of the composite A359/SiCp and 6061/Al_2O_3p. The objectives of the research were to:

1. Implement the ductile-regime machining technique to both the matrix metal and the reinforcing ceramic for a high quality surface
2. Study the wear of both polycrystalline diamond (PCD) and single-crystalline diamond (SCD) tools
3. Compare the surface integrity of ultraprecision machined and ground MMCs.

LITERATURE REVIEW

There were limited published papers on ultraprecision machining of MMCs, and on ductile-regime machining of brittle materials. When a material was machined in such a fine scale that satisfied ductile-regime conditions, then the chip was removed in a ductile manner despite the brittle nature of the material. A model for the critical depth associated with ductile-regime in micromachining was proposed (6):

$$d_c \alpha \frac{\text{plastic flow energy}}{\text{fracture energy}} = A\left(\frac{E}{H}\right)\left(\frac{K_{cs}}{H}\right)^2 \tag{1}$$

Where

d_c : critical depth of machining
E : Young's modulus
K_{cs} : critical surface fracture toughness
H : material hardness
A : constant, depending on the environment and cutting conditions.

A shallow depth of cut, therefore, would energetically promote plastic flow rather than brittle fracture in the substrate and the chips. Using equation (1), the critical depth of cut, d_c, for Si, SiC, and Al_2O_3 were calculated to be 0.4, 0.6, and 1.0 μm respectively. Further investigation showed that grinding speed had insignificant effect on d_c, but there was a dramatic change of d_c when using water or alcohol as grinding fluids. The study suggested that such change was due to a chemical reaction that modified the surface properties of the materials. This hypothesis was proven by a later study in which different cutting fluids were systematically utilized to modify the surface properties of the work pieces (7). A new variable called the ζ-potential was introduced. This potential, dependent on the work piece material and the cutting fluid, measured a voltage causing by the charges in the solution of a given liquid-solid interface. By scratching, indenting, and grinding glass in a micro scale, the proportional constant A in equation (1) was found to be 0.15. Since there was a chemical effect that altered the hardness and fracture toughness at the surface, variation of the critical depths of machining was expected. By experimenting with different types of alcohol and water when machining glass, the study found the ζ-potential should be zero to promote ductile-regime machining. The same chemo-mechanical effect, to promote ductile-regime machining in micromachining, could be used to improve machining efficiency in macromachining, which was characterized by the dominating brittle fractures.

Ultraprecision machining of as-cast and extruded 6061/SiCw was studied (8). The MMCs were machined with SCD tools at pre-selected depths of cut in the range of 10-40 μm. Higher speed, lower feed, shallower depth of cut, and low volume fraction of reinforcement improved the surface finish of the samples. Further study using transmission electron microscopy (TEM) showed the high-density dislocation in the soft aluminum matrix below a machined surface. The reinforcing SiC whiskers were either "cut directly," rotated, or pulled out during the machining process.

Milling and grinding of aluminum-based MMCs reinforced with SiC or Al_2O_3 particles/whiskers were evaluated (9). Depth of cut was selected at 15μm. Examination of the machined surfaces by electron microscopy showed brittle fractures and evidences of pulled-out reinforcements. Grinding of A359/SiCp and 2618/Al_2O_3p were also experimentally performed (4, 10, and 11). Fine grinding using a 3000-grit diamond wheel at 1 μm depth produced ductile-regime cutting of the Al_2O_3 particles but micro fracture on the brittle SiC particles.

Other authors had recognized the influence of crystal orientations when investigating the ductile-regime machining of other brittle materials such as silicon

(12–14) and germanium (15). Silicon wafers with a (111) crystallographic plane at the wafer surface were machined with diamond tools at different machining parameters and conditions. Both feedrate and depth of cut must be kept below some thresholds to guarantee a ductile-regime machining. Negative rake tools provided a hydrostatic stress field in the material just below the tool, and prevented brittle fracture from occurring (12, 13, and 15). The direction of cutting relative to the crystal orientation also contributed to the different chip removal mechanisms. A mirror like surface was obtained when cutting along the <110> direction. The critical depth of cut was 140 nm when cutting along the $[2\bar{1}\bar{1}]$ direction, but increased to 153 nm for the $[11\bar{2}]$ direction (12). Other authors ultraprecision machined the (001) wafers and found different results for cutting along different directions (13). Kerosene was used as coolant and lubricant together with a single crystal diamond tool for the ultraprecision facing operation. At a depth of cut of 1 μm, about 50% of the ductile regime was seen when cutting along the $[\bar{1}00]$ direction, but nearly 100% ductile regime was seen along the $[\bar{1}\bar{1}0]$ direction when the depth of cut was reduced to 0.1 μm. When machining the (111) silicon wafers, an almost 100% ductile regime was seen for all directions at an 0.1 μm depth of cut. Dependence of cutting direction was seen for 1 μm depth of cut. The model was proposed and later verified that ductile regime machining was realized when more slip systems were activated.

A different approach was used to evaluate the critical depth of cut (15). By quickly withdrawing a cutting tool and subsequently inspecting the uncut shoulder, the authors visually measured the critical chip thickness and its location. When cutting the (100) germanium with a single crystalline diamond tool, the critical thickness changed from 0.13 μm to 0.29 μm when machining in distilled water and air, respectively. Negative rake angle and large tool nose radius improved the machinability.

Simulation using the molecular dynamic technique was accomplished (14). Two criteria for chip removal were discussed: (i) for brittle fracture, the resolved tensile stress on a cleavage plane must exceed a critical value, and (ii) for ductile fracture, the resolved shear stress in a slip direction must exceed a critical value. Micro grinding, turning, and indenting showed the critical depth for silicon was about 1μm.

EXPERIMENT

The cast A359/SiC/10p and extruded $6061/Al_2O_3/15p$ composites were kindly provided by Duralcan. The former was used extensively in this study since it was more difficult to machine the SiC-reinforced MMCs. Some of the as-cast samples were hot-isostatically pressed (HIP) and/or aged to enhance the matrix properties. Tensile properties of the MMCs were measured with a tensile testing system (Instron 4206). Although no coolant was used during machining, compressed air was directed to blow the chip away from a machined surface. Both SCD and PCD tools were used for the facing operations. Tool crystalline orienta-

tion was measured using a x-ray diffractometer (Philips X'Pert-MPD). The cutting edge radius (tool edge sharpness) and surface profile were measured on an atomic force microscope (AFM, Digital Instrument Nanoscope IIIa). Table 1 provides more relevant information on the materials and cutting tools.

Short coupons of MMC samples were mounted on a precision fixture using hot melting wax (T_m = 80°C) to avoid the undesirable effects of mechanical clamping. All samples were rough faced with a PCD tool at 5 μm, then five passes at 1μm depth of cut. They were then faced two passes with a new SCD tool at 1 μm then three passes at the desired depth of cut. Both continuous and interrupted facing of short MMC coupons were performed on an ultraprecision machine (PreciTech Optimum2800) that had 2.5 nm feedback resolution and 9 nm positioning accuracy. All feedrates were normalized at 0.5% of tool nose radii. Some samples were machined at constant depths of cut at a range of 0.2–1.0 μm and at an increment of 0.2 μm. In another experiment, a cutting tool was programmed to move at an angle almost perpendicular to the rotating axis. Such a taper cut in a facing operation was necessary to vary the depth of cut continuously from 0.0 to 0.2 μm. The cutting velocity was calculated from the rotational speed in a facing operation (rpm) and the radial location at the point of interest.

Precision grinding was performed to verify the calculated machining depths. Both the A359/SiC/20p-T6 and the 6061/Al_2O_3/15p-T6 composites were surface ground on a precision grinding machine (Okamoto PSG-64DX). A diamond wheel of 3000 grit, resin bond, was used to grind at 1100, 1650, and 2200 m/min speed, at 1 μm depth of cut, 20.8 m/min feed, and 1 mm/pass cross feed.

Machined surfaces were analyzed with an AFM, a profilometer (Form Talysurf 120L), and with a scanning-electron microscope (SEM, Cambridge S360). The as-machined samples were observed/scanned directly first, then repeated again after etching the samples in Keller's etchant (190 ml H_2O, 5ml HNO_3, 3

Table 1. Details of the Composite and Cutting Tools

Materials	Matrix: Al, 9.27 wt% Si, 0.15 Fe, 0.55 Mg. Reinforcement: 10 vol% SiC particles. Aspect ratio 1.5:1. Median 9.3 ± 1.0 μm, 94% particles ≥ 3 μm, 3% particles ≥ 19μm. Processes: • Permanent-mold cast to ϕ18 mm bars. Pouring temperature 700–710°C, average stirring rate 175 rpm. • Hot isostatic pressing (HIPping) by heating in argon at 550°C for 1 hour, isostatically pressed at 150 MPa for 1 hour, oven-cooled to 300°C, then air-cooled. • Solution heat-treated at 540°C for 14 hours, water quenched, peak aged at 155°C for 5 hours to obtain the T6-temper.
Tools	Polycrystalline diamond: 0.5 μm grain size, ASA* tool geometry 0°, 0°, 9°, 5°, 60°, 30°, 0.33 mm; edge sharpness 500-750 nm. Single crystalline diamond: (100) rake plane, ASA tool geometry (±5° & 0°), 0°, 5°, 5°, 30°, 0°, 0.51-2.06 mm; edge sharpness 20-80 nm.

* American Standard Association

ml HCl, 2ml HF) to dissolve the smearing aluminum on the surfaces. Selected samples were sectioned, mounted, hand ground, polished then etched to show the microstructure at the subsurface. The Energy Dispersive X-ray (EDX) technique was used to identify different phases and elements on a sample.

RESULTS

Experimental results on tensile properties, surface integrity, ductile-regime model, and tool wear are presented and discussed next. Evidence of ductile-regime machining of the MMCs obtained by ultraprecision machining and diamond grinding are then compared.

Tensile Property

Table 2 summarizes the tensile properties of the MMCs after heat treatment and HIPping. As expected, the HIPping and aging of MMCs improved the tensile strength while maintained the ductility of the composites. Since voids are unavoidable in MMCs during casting, HIPping should (i) "heal" those vacuum-filled voids, therefore, provide a denser matrix to support the particles, and (ii) relieve the residual stress due to thermal mismatch between the aluminum matrix and the ceramic particles, therefore, improve the ductility of the annealed matrix but reduce the yield strength of the material. The yield strength of the MMC after HIPping, however, can be improved by providing the Mg_2Si precipitates in the matrix via an aging process. The respective hardness measurements of the MMC in the as-cast condition (F) and HIPped then aged condition (HIP-T6) were 71 and 92 RF, respectively. Examination of the fractured surface of MMC tensile samples by SEM did not reveal any sign of interfacial degradation due to either HIPping or aging. This agreed with the increment in tensile strength of the composite as seen in Table 2.

Analysis of the MMC microstructure showed a favorable reduction of volumetric porosity of the A359/SiC/10p from 1.2% to 0.2%. A repeated study on the A359/SiC/20p showed a reduction of porosity from 1.8% to 0.3%.

Table 2. Tensile Properties of Tested Composites (average of 3 samples)

MMCs	TENSILE STRENGTH (MPa)	YIELD STRENGTH, 0.2% OFFSET (MPa)	ELONGATION (%)
A359/SiC/10p-F	184	142	1.4
A359/SiC/10p-HIP	163	87	7.1
A359/SiC/10p-T6	280	263	0.6
A359/SiC/10p-HIP-T6	322	270	1.6

Surface Integrity

Both of the average roughness R_a, and the root-mean-square roughness R_q were used to characterize the surface finish. The surface integrity was further assessed by micro-examination of the as-machined or sectioned surfaces with or without etching.

A parallel study on ultraprecision machining of copper alloys was completed. A mirror surface with $R_a < 5$ nm was achieved using the same process parameters and tooling (Fig. 1). The analysis showed minimum impact from the material conditions and cutting speeds on the surface finish; however, the tool material significantly affected the surface finish, followed by the feedrate and tool radius (16):

$$R_a = \frac{R^2}{f}\left(2\varphi - \theta + \sin 2\varphi - \frac{1}{2}\sin 2\theta\right) + y_G - \frac{4y_G(R^2 - y_G^2)^{0.5}}{f} \qquad (2)$$

where

R_a : averaged surface finish, μm
f : feed rate, μm/rev
R : tool nose radius, μm
θ, φ, y_G : functions of f and R

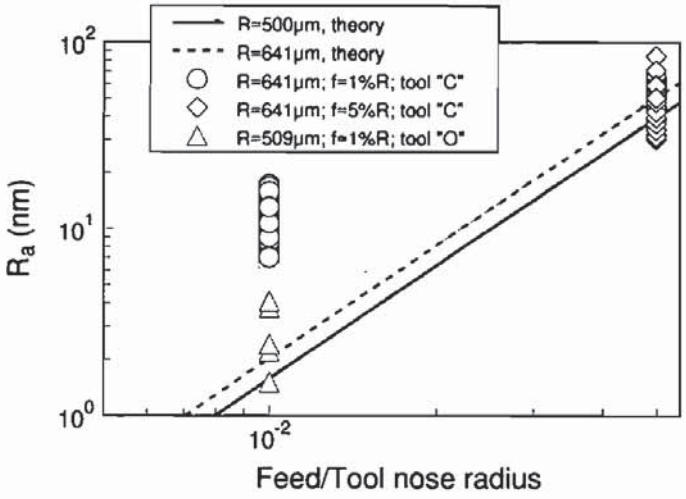

Figure 1. Comparison between theoretical and experimental surface finishes values. Dry facing of Cu-1.8wt%Be in the H and HT tempers; 75 m/min maximum speed, 0.2–1.0 μm depth, 1–5%R μm/rev feed, −25° to 5° back rake, R = 509–641 μm nose radius. Tools "O" and "C" are single crystalline and synthetic diamond tool, respectively (16).

For a small feedrate compared to the nose radius, equation (2) reduced to:

$$R_a = K(f, R)\frac{f^2}{R} \approx 0.032\frac{f^2}{R} \tag{3}$$

Since the feedrates were chosen to be 0.5% of the tool nose radii for different cutting tools, the effect of different tool nose radii should be "adjusted" for comparison purposes. The adjusted value of surface finish was derived from equation (3) as:

$$R_a' = \frac{R'}{R} R_a \tag{4}$$

where

R_a : measured surface finish
R_a' : surface finish, adjusted for different tool nose radius
R : actual tool nose radius
R' : hypothetical tool nose radius

The calculated surface finish using either equation (2) or (3) agreed with the measured surface finish for copper alloys, but not the MMCs. Shattered SiC particles and tool wear degraded the surface finish of MMC samples. Consistency of the measured results was observed when measuring the surface finish with a profilometer or an AFM (Fig. 2).

The measured results in Fig. 2 and other measurements were adjusted for different tool radii. For example, when a tool with a nose radius of $R = 2.06$ mm

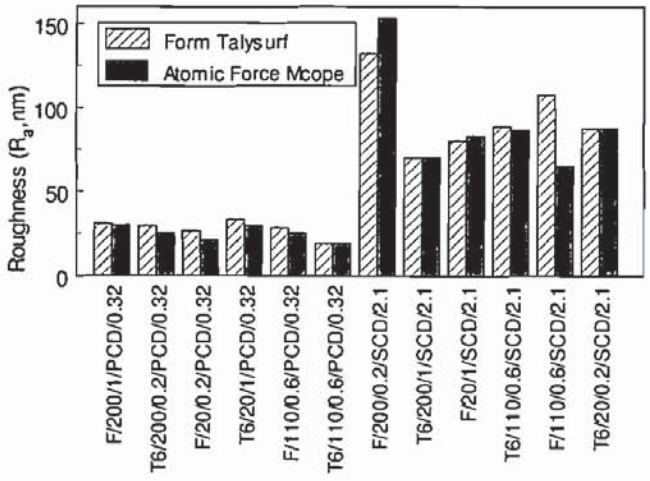

Figure 2. Comparison of surface roughness measured by different techniques. Facing A359/SiC/10p at feed = 0.5% nose radius (μm/rev). The sample's nomenclature indicates Temper, Cutting speed (m/min), Depth of cut (μm), Tool material, and Tool radius (mm).

was used to produce a surface roughness of R_a, the "adjusted" surface roughness would be R'_a if a tool of radius $R' = 0.50$ were used instead. Equation (4) gives the correction factor as the ratio of the tool radii, which is 0.50/2.06 in this example. Using the tool with 0.50 mm nose radius as the bases for comparison, the results of the best surface finish measured from the machined samples are shown in Fig. 3. Although the resolution of roughness measurement was less than 2 nm, the repeatability of measurement at different locations on a sample was as high as 25 nm. In all cases, the adjusted surface roughness is in the range of 20–50 nm R_a if machining with tools of consistent 0.5 mm radii. This range was comparable with the published range of 10–62 nm for the 6061/SiCw machining with unknown tools (8).

The effect of ultraprecision machining parameters was investigated. The surface finish of single crystal metals or semiconductors was sensitive to the environment, tooling, and machining parameters. However, the surface finish of MMCs was not that responsive in ultraprecision diamond machining. An experiment was done by facing multiple samples, which were processed at different tempering conditions and positioned with hot melting wax on a fixure at the same radial distance. All the samples, therefore, were faced with the same tool at the same cutting conditions and parameters. The results showed that surface finish measurements were indifferent for tools with ±5° or 0° rake angles; or between as-cast, HIPped, and heat treated tempers; or varying cutting speed in the range of 10-200 m/min. This was not a surprise since all the measurements were confined in

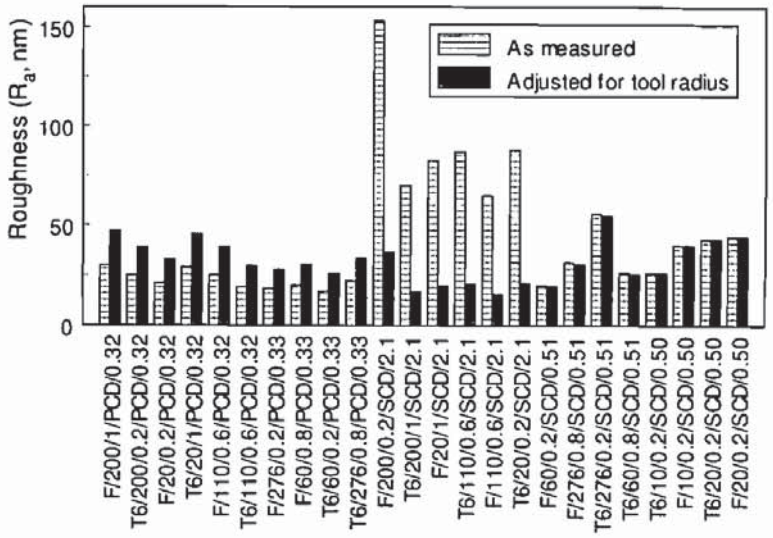

Figure 3. Measured and adjusted values of the surface roughness for 0.5 mm nose radius tools. Facing A359/SiC/10p at feed = 0.5% * actual nose radius (μm/rev). The sample's nomenclature indicates Temper, Cutting speed (m/min), Depth of cut (μm), Tool material, and Tool nose radius (mm).

Figure 4. Surface integrity of as-machined A359/SiC/10p-F after ultraprecision machining with a poly-crystalline diamond tool. The arrow points at a broken SiC particle on the surface. Cutting direction is from the bottom to the top. Facing at 276 m/min speed, 0.2 μm depth, 1.65 μm/rev feed using PCD tool (0.5 μm grain, 0° rake, 0.33 mm radius, 500–750 nm sharpness).

the aluminum phases. The surface integrity of the machined surface must be evaluated to assess the effectiveness of the process.

Examination using SEM and AFM showed that surfaces of the samples were smeared with the soft aluminum matrix, which covered most of the broken SiC particles when machined with a PCD tool (Figs. 4 and 6). The rubbing and smearing of a PCD tool were inevitable since the PCD tool edge sharpness was in the range of 0.50-0.75 μm (Table 1), that was greater than the depth of cut of 0.20 μm (Fig. 4). In contrast, different phases and more broken SiC particles in the eutectic zones were visible on MMC samples machined with a SCD tool (Figs.

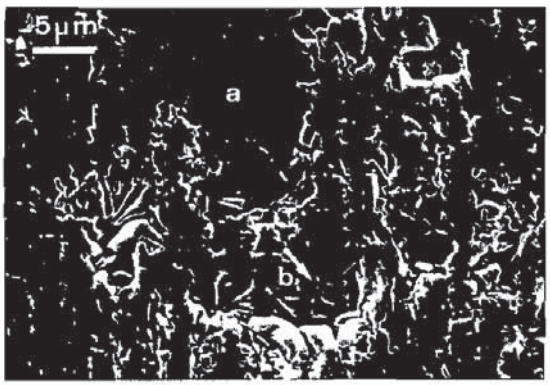

Figure 5. Surface integrity of as-machined A359/SiC/10p-F after ultraprecision machining with a single-crystalline diamond tool. Notice (a) the ductile feed marks and (b) an extending feed mark on a machined SiC particle. Cutting direction is from the top to the bottom. Facing at 0.37 m/min speed, 15 nm depth, 2.55 μm/rev feed using SCD tool (0° rake, 0.51 mm radius).

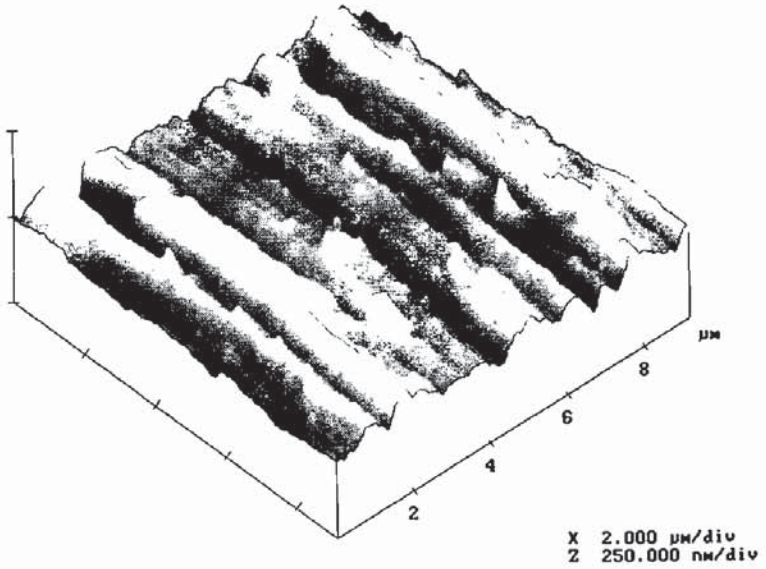

Figure 6. AFM scan of the as-machined A359/SiC/10p-HIP-T6 after ultraprecision machining with a poly-crystalline diamond tool. Facing at 20 m/min speed, 1 μm depth, 1.65 μm/rev feed using PCD tool (0.5 μm grain, 0° rake, 0.33 mm radius, 500–750 nm sharpness).

5 and 7). Notice the different scales in Figs. 6 and 7 for different cutting tools. Recall that the feedrate was chosen to be 0.5% of the actual tool nose radius, and an AFM scan size was chosen to cover at least three feedmarks. Due to the broken silicon dendrites and SiC reinforcements in the eutectic phase, the surface roughness varied greatly depending on whether the measurement was confined within a smoother aluminum phase or in the rougher SiC-containing eutectic phase (Table 3).

Ductile-Regime Machining

Ductile regime machining of the hard SiC particles was confirmed by examining the as-machined surface, the sectioned subsurface, and the etched surfaces. At depths of cut below 0.2 μm, some SiC particles were machined in the pseudo ductile mode (Fig. 8), but some were shattered in a brittle fashion (Fig. 9). Shattering of a SiC particle by a diamond tool was probably due to deeper effective depth of cut, unfavorable orientation of that SiC particle with respect to the cutting tool, or defects in the SiC particles. A deeper effective depth of cut was possible due to minute rotation of a SiC particle when first engaged with the cutting tool. A preliminary experiment to measure the force using a high sensitive piezo-dynamometer showed that the forces were in the sub-Newton range. Although small, such cutting force might be enough to separate and rotate those partially wetted SiC particles from the matrix, thus effectively increase the depth of cut beyond

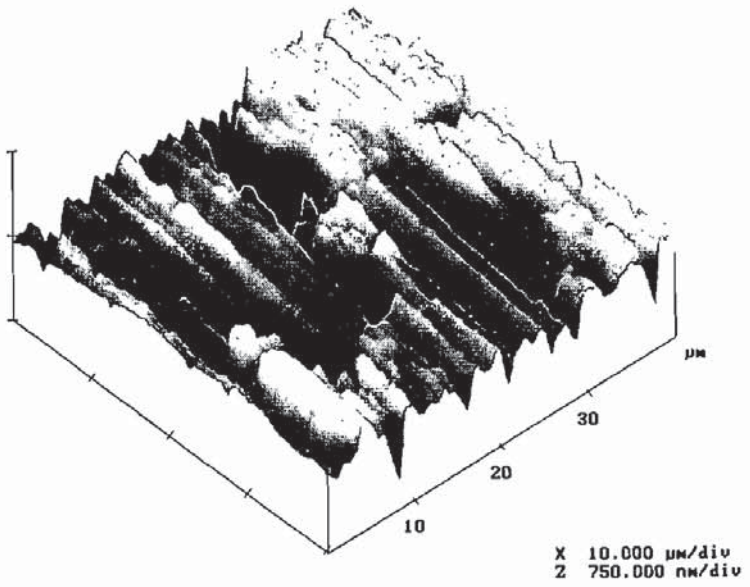

Figure 7. AFM scan of the as-machined A359/SiC/10p-HIP-T6 after ultraprecision machining with a single-crystalline diamond tool. Facing at 110 m/min speed, 0.6 μm depth, 10.3 μm/rev feed using SCD tool (0° rake, 2.06 mm radius).

the critical threshold. Plastic deformation of the matrix, loosened SiC particles from a previous cut, and defects in the particles also contributed to this problem.

The selected physical and mechanical properties, required in equation (1) for SiC are tabulated in Table 4. Thus, the calculated range d_c in equation (1) was 0.023-0.059 μm. This range for micro-scratching, however, did not agree with the published critical grinding depth 0.6 μm for SiC (6).

Grinding of the aluminum composite 6061/Al_2O_3/15p-F using fine diamond wheels at 1 μm in-feed (depth of grinding) produced visible ductile grinding marks on the Al_2O_3 particles (Fig. 10), but not on the SiC particles in the A359/SiC/20p-T6 composite. This result verified the calculated value of d_c for Al_2O_3 of 1μm

Table 3. Dependence of Surface Roughness on Measuring Locations. Facing of A359/SiC/10p-F at 0.8 μm depth, 60 m/min speed, 1.65 μm/rev feed using PCD tool (0.5 μm grain, 0° rake, 0.33 mm radius, 500-750 nm sharpness).

	PARAMETER	PLANE ROUGHNESS	SECTIONAL ROUGHNESS
Matrix	R_a (nm)	14.2	19.9
	R_q (nm)	25.3	
Eutectic	R_a (nm)	47.2–54.6	27.13
	R_q (nm)	60.9–73.7	

Figure 8. Pseudo-ductile mode of SiC particle. Notice (a) the ductile feedmarks, and (b) the microcleavages. Cutting direction is from the top to the bottom. Facing A359/SiC/10p-F then etching with Keller's etchant. Ultraprecision machining at 9.6 m/min speed, 2.55 μm/rev feed, 0.2 μm depth of cut using SCD tool (0° rake, 0.51 mm radius).

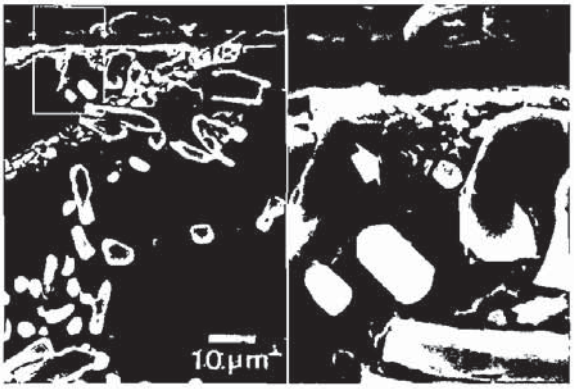

Figure 9. Subsurface of ultraprecision machined A359/SiC/10p-HIP-T6. The arrow points at the fractured SiC particle below the machined surface. Facing at 20 m/min speed, 10 μm/rev feed, 0.2 μm depth of cut using SCD tool (0° rake, 2.0 mm radius). Cutting direction is from the left to right.

Table 4. Selected Properties of Common Reinforcements for MMCs (17)

CERAMICS	YOUNG'S MODULUS (GPa)	FRACTURE TOUGHNESS ($MPa.m^{0.5}$)	KNOOP HARDNESS (GPa)
α-Al_2O_3	275–393	3.85–5.90	19.6–20.1
SiC	382–475	2.50–3.50	24.5–25.0

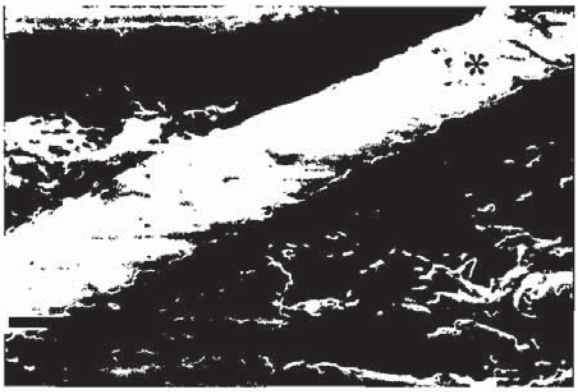

Figure 10. Ductile-regime grinding of 6061/Al_2O_3/15p-T6. Notice the horizontal grinding mark on the Al_2O_3 particle (labeled *). Surface grinding with 3000-grit diamond wheel, resin bond, 1100 m/min, 1 μm depth.

(6). Using the properties of Al_2O_3 in Table 4 and d_c = 1 μm, equation (1) gave the value of the constant $A \approx 0.6$. With this new constant A, the adjusted critical depth of cut for SiC should be in the range of 0.092–0.236 μm. This result agreed with the experimental depth of cut 0.2 μm at which the transition of ductile-brittle machining of SiC was observed (Fig. 8). The equation (1), therefore, should be modified as following for ultraprecision machining of MMCs reinforced with either SiC or Al_2O_3 reinforcement:

$$d_c = 0.6\left(\frac{E}{H}\right)\left(\frac{K_{cs}}{H}\right)^2 \tag{5}$$

Since crystallographic orientations affected the critical depth of cut of semiconductor materials (12-15), it was reasonable to assume that ductile-regime machining of SiC was also affected by the crystalline orientation as well as its physical and mechanical properties. The SiC reinforcement had either diamond structure (β-SiC), hexagonal or rhombic structure (α-SiC). The critical resolved shear stress, on a crystalline plane of SiC due to the cutting action, was directly proportional to the Schmid factor $\cos\lambda\cos\phi$, where ϕ and λ were the orientations of the slip plane and slip direction. It was postulated that an ideal ductile mode happened when the cutting shear stress was parallel to both the slip plane and the slip direction, otherwise a pseudo ductile mode with micro cleavages was seen. Equations (1) and (5), therefore, lacked the contributing factor of the crystalline orientation. This probably was the principle reason for the variation of published critical depths for ductile-regime machining of SiC. Since random distribution of SiC particles in a cast MMC was obtained, it was impractical to characterize or control the crystalline orientation of all these micro particles. This explained why some particles, on the same machined surface, were ductile-regime machined (Fig. 8) but others were machined with micro cleavages or even fractured (Fig. 9).

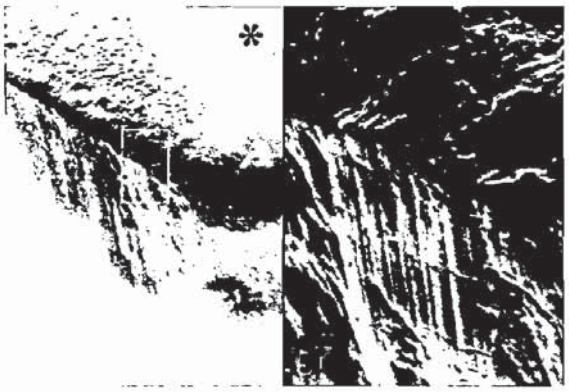

Figure 11. Distinctive abrasive wear on poly-crystalline diamond tool. The symbol "*" indicates the tool rake face. Dry facing A359/SiC/10p-T6 after 1 hr, 420 m/min maximum speed, 1.65 μm/rev feed, 0.2–1.0 μm depth of cut using PCD tool (0.5 μm grain, 0° rake, 0.34 mm radius).

Machining at a depth of cut below the critical threshold, as predicted in equation (5) was the only necessary condition for ductile-regime machining. Thus, it was very difficult to obtain the true ductile-regime turning of MMCs reinforced with particles or whiskers.

Wear of Single- and Poly-Crystalline Diamond Tools

Scanning electron microscopy (SEM) examination showed expected abrasive wear of the PCD tool (Fig. 11), but surprising and substantial wear of the SCD tool (Fig. 12). Similar results were seen for all other SCD tools. Because the pitch of the wear surface in Fig. 12 was roughly the same as the feedrate of

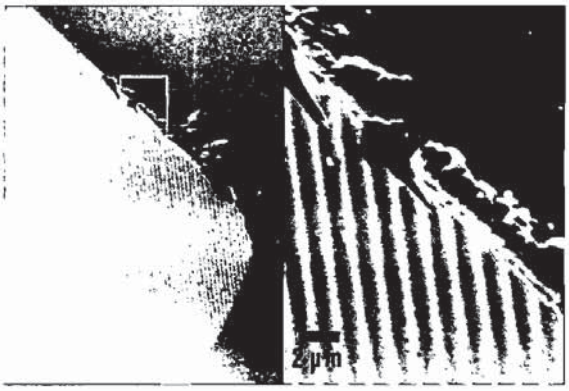

Figure 12. Excessive abrasive wear on single-crystalline diamond tool. Notice the chipping at the cutting edge, and the vertical feed marks on the tool. The symbol "*" indicates the tool rake face. Dry facing A359/SiC/10p after <1 hr, 420 m/min maximum speed, 2.5 μm/rev feed, 1.0 μm maximum depth of cut. SCD tool (0° rake, 0.5 mm radius).

2.5 μm/rev, the diamond had the characteristic of a "very soft" material. Since such excessive wear of SCD was similar to the diffusive and abrasive wear of diamond when machining or rubbing against steel (18), it was postulated that a combination of diffusive and abrasive wear mechanisms of SCD was possible when machining MMCs containing SiC. A preliminary investigation with ultraprecision machining of 6061/Al_2O_3/20p, however, did not show similar wear on a similar SCD tool.

CONCLUSIONS

Ultraprecision machining of A359/SiC/10p was studied, and conditions for ductile-regime turning for both the matrix and the reinforcement were sought. This investigation showed:

1. Pseudo ductile-regime machining of SiC particles was found. A depth of cut below 0.2 μm was the only necessary condition for ductile-regime machining. A modified model was proposed for predicting the critical depth of machining for MMCs reinforced with Al_2O_3 or SiC. A complete model should include the crystallographic orientation of the reinforcement.
2. The blunt cutting edge of the PCD tool rubbed and smeared the aluminum on the machined surface, but the sharp cutting edge of the SCD tool cut the surface effectively to reveal different phases.
3. The resulting surface finish was not significantly affected by the tool materials, the material temper conditions, and machining parameters when ultraprecision machining at a depth of cut below 1μm.
4. Abrasive wear of the PCD tools was seen, but a suspected diffusive-abrasive wear of the SCD tools was observed.

ACKNOWLEDGMENT

The authors would like to thank Duralcan for the composites, Sumitomo and Osaka Diamond for the cutting tools. The study was funded from the NTU research grant RG 62/95.

REFERENCES

1. N.P. Hung, F.Y.C. Boey, K.A. Phua, and H.F. Lee, "Machinability of Aluminum Alloys Reinforced with SiC Particulates," *J. Materials Processing Technology*, 56 (1996) 966–977.
2. N.P. Hung, L.J. Yang, and K.W. Leong, "Electrical Discharge Machining of Cast Metal Matrix Composites," *J. Materials Processing Technology*, 44 (1994) 229–236.
3. N.P. Hung, S. Jana, L.J. Yang, and C.H. Heng, "Laser Drilling of Cast Metal Matrix

Composites," *Proceedings on Machining of Advanced Materials* , ASME AMD 208, Los Angeles, (1995) 87–92.

4. N.P. Hung, Z.W. Zhong, and C.H. Zhong, "Grinding of Metal Matrix Composites Reinforced with Silicon-Carbide Particles," *J. Materials and Manufacturing Processes*, 12 (6) (1997) 1075–1091.
5. N.P. Hung, C.M. Yoong, and B.H. Low, "Abrasive Blasting of Metal Matrix Composites," *J. Materials and Manufacturing Processes*, 13 (1) (1998) 101–115.
6. T.G. Bifano, T.A. Dow, and R.O. Scattergood, "Ductile-regime Grinding of Brittle Materials: Experimental Results and the Development of a Model," *Advances in Fabrication and Metrology for Optics and Large Optics*, SPIE 966, (1988), 108–115.
7. T.G. Bifano, D.K. DePiero, and D. Golini, "Chemomechanical Effects in Ductile-regime Machining of Glass," *J. Precision Engineering*, 15(4) (1993) 238–247.
8. Z.J. Yuan, L. Geng, and S. Dong, "Ultraprecision Machining of SiCw/Al Composites," *Annals of the CIRP*, 42(1) (1993) 107–109.
9. H. Chandrasekaran and J.O. Johansson, "Influence of Processing Conditions and Reinforcement on the Surface Quality of Finish Machined Aluminum Alloy Matrix Composites," *Annals of the CIRP*, 46(1) (1997) 493–496.
10. Z.W. Zhong, N.P. Hung, N.L. Loh, and T. Sano, "Grinding of Aluminum-Based Metal Matrix Composites," *Proc. of the International Conference on Mechanics of Solids and Materials Engineering*, Singapore, A (1995) 274–279.
11. N.P. Hung, Z.W. Zhong, and C.H. Zhong, "Grindability of Metal Matrix Composites," *Proc. of the Fourth Conference on Composites Engineering*, Hawaii, (1997) 459–460.
12. T.P. Leung, W.B. Lee, and X.M. Lu, "Diamond Turning of Silicon Substrates in Ductile Regime," *J. Materials Processing Technology*, 73 (1998) 42–48.
13. T. Shibata, S. Fujii, E. Makino, and M. Ikeda, "Ductile-Regime Turning Mechanism of Single Crystal Silicon," *J. Precision Engineering*, 18(2/3) (1996) 129–137.
14. S. Shimada, N. Ikawa, T. Inamura, N. Takezawa, H. Ohmori, and T. Sata, "Brittle-Ductile Transition Phenomena in Microindentation and Micromachining," *Annals of the CIRP*, 44(1) (1995) 523–526.
15. W.S. Blackley and R.O. Scattergood, "Ductile-regime Machining Model for Diamond Turning of Brittle Materials," *J. Precision Engineering*, 13(2) (1991) 95–103.
16. N.P. Hung and Z.W. Zhong, "Ultraprecision Machining of Copper Beryllium Alloys," *Proceedings of the 6th International Conference on Processing and Fabrication of Advanced Materials*, Singapore, (1997).
17. E. Ratterman and R. Cassidy, "Abrasives," *Engineering Materials Handbook: Ceramics and Glasses*, ASM, 4 (1991) 329–335.
18. J. Wilks, and E. Wilks, *Properties and Applications of Diamond*, Butterworth & Heinemann, Boston, (1991) 348–356.